A new technique for angle-dispersive powder diffraction using an energy-dispersive setup and synchrotron radiation

Yanbin Wang, Takeyuki Uchida, Robert Von Dreele, Mark L. Rivers, Norimasa Nishiyama, Ken-ichi Funakoshi, Akifumi Nozawa and Hiroshi Kaneko

A new technique for angle-dispersive powder diffraction using an energy-dispersive setup and synchrotron radiation

Yanbin Wang,[a]* Takeyuki Uchida,[a] Robert Von Dreele,[b] Mark L. Rivers,[a] Norimasa Nishiyama,[a] Ken-ichi Funakoshi,[c] Akifumi Nozawa[c] and Hiroshi Kaneko[d]

[a]Center for Advanced Radiation Sources, The University of Chicago, USA, [b]APS/IPNS, Argonne National Laboratory, USA, [c]Japan Synchrotron Research Institute, Japan, and [d]Japan Atomic Energy Research Institute, Japan. Correspondence e-mail: wang@cars.uchicago.edu

A new diffraction technique for combined angle- and energy-dispersive structural analysis and refinement (CAESAR), by collecting angle-dispersive data using a solid-state detector (SSD) and white synchrotron radiation, is introduced. By step scanning a well calibrated SSD over a limited 2θ range, a series of one-dimensional energy-dispersive data (intensity *versus* energy) are obtained as a function of 2θ. The entire intensity (Int) data set consists of several thousand channels covering a range of photon energies, E (up to $\sim$150 keV), at each of the $\sim$1000 2θ steps, forming a 2–4 mega-element two-dimensional array, Int(E, 2θ). These intensity data are then regrouped according to photon energies, which are defined in the multichannel SSD as individual channels, yielding a large number of intensity *versus* 2θ (angle-dispersive) data sets, Int(E = const., 2θ), each of which corresponds to a given photon energy or wavelength. The entire data set, selected subsets or composite scans can be used for multiple data set Rietveld refinement. Data collected both on α-Al_2O_3 (a NIST diffraction standard) at ambient conditions and on a mixture of MgO and Au at high pressure were analyzed using the Rietveld technique, with varying schemes of data treatment. Furthermore, it is demonstrated that data within certain energy bands ($\Delta E/E = \pm 10\%$) may be binned together to improve counting statistics in a composite angle-dispersive scan, even when collected with much coarser scan steps of 0.1 or 0.2°. This technique is useful for high-pressure as well as general purpose powder diffraction studies that have limited X-ray access to the sample using synchrotron radiation. Several advantages are discussed.

1. Introduction

Many materials undergo structural phase transformations under pressure and temperature. Crystal chemistry of high-pressure and high-temperature phases and structures of liquids and amorphous materials are of great interest to solid-state physics, materials science and geophysics. However, limited X-ray access in a pressure device or a high-temperature vessel often compromises data quality. As a result, previous high-pressure studies were often limited to the energy-dispersive diffraction (EDD) technique, carried out at a fixed 2θ angle. The data collection is fast (of the order of minutes or seconds), and the incident and diffracted beams can be well collimated such that clean diffraction data can be obtained even in the presence of pressure media surrounding the sample. The EDD diffraction information is useful in phase identification and determination of unit-cell volume but does not provide reliable crystal chemistry information, such as bonding characteristics and atomic positions. Various

efforts have been made to extract quantitative crystallographic information from EDD data, with limited success (*e.g.* Yamanaka & Ogata, 1991; Yamanaka *et al.*, 1992; Ballirano & Caminti, 2001). Difficulties encountered include appropriate descriptions of the variation in incident intensity and absorption within the experimental environment. In studies of liquids and amorphous materials, EDD data are collected at multiple 2θ angles, in order to increase reciprocal-space coverage for a more accurate determination of the radial distribution functions (*e.g.* Urakawa *et al.*, 1996).

On the other hand, numerous attempts have been made to perform monochromatic diffraction using various high-pressure devices. For example, step-scan angle-dispersive diffraction (ADD) studies have been carried out using the multianvil press (MAP). In these experiments, a monochromator is used to select a photon energy for the incoming radiation, and a point detector (sometimes with a crystal analyzer) is scanned at a given step size in 2θ to collect diffracted intensity as a function of 2θ (*e.g.* Zhao *et al.*, 1994). The higher data quality

achieved is at the cost of throwing away a vast majority (> 99.9%) of photons at other energies and most of the diffracted photons at the same energy, at angles not covered by the detector scan path. Because of the relatively weak monochromatic beam intensity, each scan may take hours to complete. In addition, the limited X-ray access imposed by the pressure vessel often restricts the 2θ range to below $15°$. For a typical photon energy of 50 keV, the coverage in d spacing is limited to above 0.95 Å, not enough to allow robust structural refinement. Higher-energy monochromators are costly and technically more challenging. Virtually no monochromators are currently available for photon energies above $\sim$100 keV.

To facilitate faster data collection and overcome problems due to sample graininess, two-dimensional X-ray detectors are used in both the MAP and the diamond anvil cell (DAC). However, an immediate compromise is the loss of diffracted beam collimation. Diffraction of the pressure media, gaskets, pressure marker *etc.*, as well as Compton scattering of the diamonds, all contribute to the background, reducing signal-to-noise ratio, sometimes severely overlapping with sample diffraction signal and affecting data quality [*e.g.* see Angel *et al.* (2000) for a review]. The advantage of the two-dimensional detector is its data collection speed. A few seconds of exposure will be sufficient to obtain diffraction data at brilliant third-generation synchrotron sources. The drawback, however, is that angular resolution may be degraded when intensities at various azimuth angles are integrated.

To overcome the background problem, a Soller slit system can be used, which consists of multiple collimators that are in a radial alignment, centered at the sample (*e.g.* Yaoita *et al.*, 1997; Schulze & Kleuker, 1998). By oscillating the Soller slits between the sample and the two-dimensional detector, background scattering can be significantly reduced in the ADD patterns thus obtained. However, accurate alignment of the Soller slits is known to be difficult.

The advent of synchrotron radiation has provided us with a brilliant X-ray source with a wide range of photon energies. Thus, an ideal diffraction technique should take full advantage of the wide energy spectrum of a synchrotron source, with simultaneous multiple ADD data collection. To this end, we present test results of a new technique for combined angle- and energy-dispersive structural analysis and refinement (CAESAR), which employs simultaneous angle- and energy-dispersive diffraction. By scanning the multichannel SSD with energies carefully calibrated, a large number of EDD patterns are obtained. The entire data set can then be rearranged as ADD patterns, by selecting intensities of each channel (a given photon energy or wavelength) as a function of 2θ. Subsets of the data covering certain narrow energy bands may be combined to give ADD patterns with improved counting statistics; these may be combined in a multipattern Rietveld analysis to utilize the entire data set efficiently. We show that this technique is able to provide good quality ADD data over a wide range of continuous photon energies. The high photon-energy data provide coverage at the low d-spacing end, where intensities are important for atomic position determination; the low photon-energy data cover the high d-spacing end,

where the large d spacing constrains cell parameter accuracy. We use diffraction data collected at two third-generation synchrotron sources (Advanced Photon Source, USA, and SPring-8, Japan), on powdered corundum, to demonstrate the feasibility of this technique and discuss further developments in applying this technique to various high-pressure vessels. Although the original goal was to develop this technique for high-pressure research, we emphasize that this technique is also applicable to general synchrotron-related diffraction studies.

2. Experimental setup

2.1. Test setup at GSECARS, APS

The first test was conducted at the insertion-device beamline (13-ID-D) of GSECARS, Advanced Photon Source (APS), under ambient conditions. The experimental setup is described by Wang *et al.* (2000).

The sample was NIST standard α-Al_2O_3 (SRM674a), with an average grain size of $\sim$2 µm. Powders were hand packed in a $3 \times 10 \times 5$ mm rectangular volume between a pair of WC blocks ($10 \times 10 \times 10$ mm) and sealed with Kapton tape. The sample was mounted on the 1000 ton multianvil press, which was held by a four-axis supporting frame, capable of moving the 7 ton press in three orthogonal directions and rotation about the vertical axis (Wang *et al.*, 2000). The sample was oriented such that the longest dimension was parallel to the incident X-ray.

The Ge SSD with a multichannel analyzer (MCA) was calibrated against several radioactive isotopes, *viz.* Co^{57}, Cd^{109}, with the following characteristic lines: weighted average of Ag $K\alpha_1$ and $K\alpha_2$ (22.104 keV), Pb $K\alpha_2$ (72.794 keV), Pb $K\alpha_1$ (74.956 keV), Cd^{109} γ_1 (88.040 keV), Co^{57} γ_2 (122.061 keV) and Co^{57} γ_3 (136.474 keV). A linear fit of channel numbers to these energies results in an accurate fit with typical uncertainties of about 5 eV around 22 keV and less than 10 eV near 136 keV. The detector energy resolution, as measured by the FWHM, was about 160 and 500 eV at 22 and 136 keV, respectively. An amplifier with shaping time of 2 µs was used.

A five-axis detector support, consisting of three linear translation and two rotation axes, was used to scan the SSD along a spherical surface, the radius of which was prescribed (Wang *et al.*, 2000). Although the detector mount is capable of scanning 2θ in any direction, for the current test we only performed a vertical scan to demonstrate the feasibility of the CAESAR technique. Both rotation axes were equipped with optical encoders, and the absolute angle positions were monitored on the basis of the encoder readout. However, scan tests of the nominal stepper motor 2θ against encoder readout showed periodic deviations, indicating that the accuracy of the drive system 2θ was no better than $\pm 0.015°$. This inaccuracy is mostly due to gearing imperfection, resulting in an oscillation with a period of roughly $2°$. Multiple scan tests indicated that these oscillations were reproducible to within $0.002°$. Because the mechanical 2θ deviated from the true 2θ, the detector

pointing position also oscillated in the direction parallel to the incident beam. This was the main reason for the choice of the large sample size used in our test. Future development in servo-control will be needed to improve pointing accuracy to a level suitable for high-pressure high-temperature crystallographic studies.

The scans were performed at 0.01° steps from 3 to 12°; each data collection took 60 s and total data collection required ~15 h. The incident beam was collimated to 0.2 × 0.1 mm (H × V), and the collimator on the diffraction side was 0.5 × 0.05 mm. Each EDD pattern consisted of 2048 energy bins, from 19 to 142 keV with a bin width of about 59.8 eV, and the entire data set was collected in 900 2θ steps.

2.2. Test setup at SPring-8

The second ambient test was performed at the bending-magnet beamline BL04B1 of SPring-8. In this test, NIST SRM 675a corundum was packed in a glass vial with an outer diameter of about 8 mm. The test was performed using the 1500 ton multianvil press SPEED-1500 (Utsumi *et al.*, 1998) and its X-ray detection system. This facility has a virtual 2θ arm consisting of two arched rails, lying in the horizontal plane, with rotation centers coinciding with the vertical center of the press. A Ge SSD slides on the rails, with a collimator pointing at the sample located at the center of the press. The rails were optically encoded to allow an accurate detector scan. Other experimental details are similar to those for the procedure performed at the APS, except that the detector was scanned in the horizontal plane, perpendicular to the cylindrical axis of the sample.

The multichannel Ge SSD was calibrated against Co^{57}, Cd^{109} and Am^{204} in a way similar to that described above for the GSECARS setup, with weighted average of Ag $K\alpha_1$ and $K\alpha_2$, Ag $K\beta_1$ (24.9424 keV), $K\beta_2$ (25.4564 keV), Am γ_1 (59.5370 keV), Cd^{109} γ_1, Co^{57} γ_2 and Co^{57} γ_3. A linear fit of channel numbers to these energies resulted in an accurate fit with typical uncertainties less than 10 eV. The detector energy resolution was very similar to that observed at the APS. The amplifier shaping time was 4 μs.

The incident beam was collimated to 0.05 × 0.5 mm (H × V), and the collimator on the diffraction side was 0.05 × 2.0 mm. The vertical beam size was chosen so that detector dead time was below 5% throughout data collection. The scans were performed from 3 to 12° with a 0.01° step size, with a collection time of 50 s at each step; total data collection required ~12.5 h, but some minor software problems prolonged the collection to about 15 h. There were 4096 energy bins in each EDD spectrum, covering energies from 0.768 to 160.917 keV with a bin width of 39 eV.

Further to demonstrate the feasibility of this technique at high pressures, we conducted a high-pressure test using a sample assembly modified from that described by Uchida *et al.* (2001), with amorphous boron as the pressure medium. SPEED-1500 is a double-stage multianvil apparatus (Utsumi *et al.*, 1998). The first-stage WC anvils and their locating rings are slotted so that a *ca* 10° range is available for 2θ access. The

second-stage anvil assembly consists of eight sintered diamond cubes with 14 mm edge length. Each cube has a triangular truncation with an edge length of 2 mm. An octahedral cavity is formed when the eight cubes are compressed by the first stage, compressing the octahedral sample assembly.

Because the virtual goniometer scans 2θ horizontally through the gaps between the second-stage anvils, we oriented the cylindrical sample chamber vertically, so that its axis was perpendicular to the diffraction vector. This approach ensured minimum variation in diffracting volume during a 2θ scan. A mixture of MgO (Alfa; grain size less than 10 μm and purity 99.998%) and Au (Alfa; grain size about 5 μm and purity higher than 99.96%) was loaded in the sample chamber, with a sample diameter of 1 mm. The sample was compressed to a maximum load of 250 tons and the step-scan test was conducted after releasing the load to 100 tons. The pressure was 8 GPa based on the unit-cell volume reduction of MgO and Au (Speziale *et al.*, 2001; Shim *et al.*, 2002). Step scans were performed from 3 to 9° with a 0.01° step size, with a collection time of 50 s at each step; total data collection required ~8 h. There were 4096 energy bins in each EDD spectrum, covering energies from 0.77 to 160.92 keV with a bin width of 39 eV. Details of the high-pressure test are given elsewhere (Wang *et al.*, 2004).

3. Results

3.1. Overview of the raw data

For each test, the entire EDD data set is combined to form a two-dimensional array of intensities, $Int(E, 2\theta)$, each Int value corresponding to a given E (photon energy) and 2θ index. Fig. 1 shows the raw data collected using the GSECARS setup at the APS. During the data collection, the undulator gap was tapered from 20 to 18 mm over its 2.5 m length, in order to generate a semi-white spectrum. The input spectrum had notable intensity modulation as a function of photon energy, which can be seen as the horizontal modulating background stripes in Fig. 1(*a*) and the 'wavy' background in the EDD patterns shown in Fig. 1(*b*). The diffraction peak intensities also oscillated with energy, riding on the undulating background. However, along a constant energy line, the background remains quite flat. The wavy undulator background structure can be minimized by closing the gap (minimum undulator gap is about 12 mm). The detector dead time was kept under 3%. The synchrotron ring current was maintained at 102 mA by regular injections throughout the scan, and therefore no input intensity correction was needed for a given energy.

Some additional lines can be seen in Fig. 1(*a*), which are more pronounced at low energies and low 2θ angles. According to Bragg's law,

$$\lambda = 2d \sin\theta, \tag{1}$$

where λ is the wavelength of the radiation, any diffraction line that satisfies (1) should follow the constant $1/(2E\sin\theta)$ [or $\lambda/(2\sin\theta)$] relation. These additional lines do not follow this

Yanbin Wang *et al.* · A new technique for powder diffraction

requirement; rather, they are shifted from the intense sample diffraction peaks by a constant increment in MCA channels (or energies). These are the Ge escape peaks, which occur
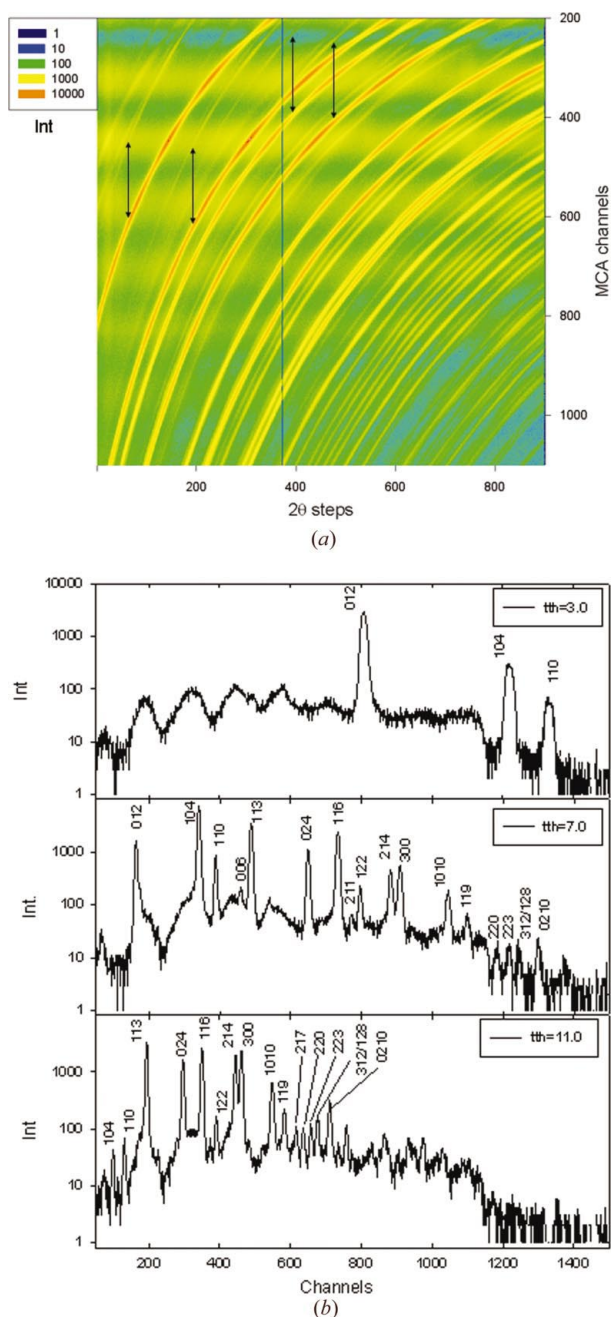

(a)

(b)

Figure 1
(*a*) A plot of intensity collected on Al_2O_3 at the APS against MCA channel numbers and 2θ steps (step 0 corresponds to $2\theta = 3°$, step size = $0.01°$). A missed step in 2θ scan is also evident (the dark line just below 400 2θ steps). The horizontal 'wavy' background stripes are due to the tapered undulator source intensity variation with energy [see (*b*)]. This background is normally a problem in ED data as peak intensities will be strongly influenced. However, along a constant energy line, the background is virtually constant. For clarity, only the data between MCA channels 200 and 1100 are shown, corresponding to photon energies from 32 to 86 keV. Double-headed arrows tie the Ge escape peaks to their parent peaks. (*b*) Selected EDD spectra at various 2θ angles obtained with a tapered undulator at the APS. Note the 'wavy' background characteristic of the tapered undulator source spectrum [see the 'wavy' background in (*a*)].

when an X-ray excites a Ge atom in the detector and the resulting Ge $K\alpha$ fluorescent X-ray ($K\alpha_1 = 9.886$ keV and $K\alpha_2 = 9.855$ keV) manages to escape the detector crystal. Some of the relatively intense escape lines are tied by the double-headed arrows to their parent diffraction lines in Fig. 1(*a*). These escape lines sometimes can cause confusion in EDD data analysis, but they are easily identifiable in two-dimensional plots.

The top panel of Fig. 2(*a*) plots the ambient data obtained at SPring-8 in two dimensions. The 2θ steps are identical to data collected using the APS undulator, whereas the MCA channels plotted in Fig. 2(*a*) correspond to energies from 36 to 141.5 keV. There are fewer escape lines [tied to the parent reflections by double-arrow-headed lines in Fig. 2(*a*)]. Note the relatively smooth bending magnet background and overall lower intensity. Unlike the APS undulator, the SPring-8 ring current had a slow decay from 100 to ∼80 mA between injections, which occurred at 12 h intervals (Fig. 2*a*, bottom panel). This decay caused the abrupt intensity changes around 2θ steps of 200 and 860. It is possible to correct for this I_0 change by rescaling the intensities. However, in the analyses presented below, this variation is simply ignored. Improvement of fitting results is expected when the I_0 corrections are applied.

Also note two consistently higher intensities around channels 1844 and 1899, which are the fluorescence peaks Pb $K\alpha_2$ (72.794 keV) and Pb $K\alpha_1$ (74.956 keV). A weaker line (Pb $K\beta$, 84.9 keV) can also be seen around channel 2150. These Pb lines are primarily from the Pb beam stop that protected the detector from the direct beam. They generally cause overlap with diffraction peaks in an EDD spectrum, contaminating the data. However, in an ADD plot, these lines only contribute to a higher flat background. This fact is demonstrated in Fig. 2(*b*), which plots intensity *versus* 2θ at 74.96 keV, the energy of the Pb $K\alpha_1$ fluorescence line.

Fig. 2(*c*) shows the data obtained at high pressure. The consistently higher intensities around channels 1694, 1741, 1843 and 1898 correspond to the fluorescence lines Au $K\alpha_2$ (66.9895 keV), $K\alpha_1$ (68.8037 keV), Pb $K\alpha_2$ (72.794 keV) and Pb $K\alpha_1$ (74.956 keV), respectively. Additional weaker lines, Au $K\beta_2$ (80.03 keV) and Pb $K\beta$ (84.9 keV), can also be seen around channels 2035 and 2150, respectively.

Figs. 1(*a*) and 2(*a*) summarize such two-dimensional data. Subsets of the two-dimensional data set can be selected according to a fixed E or 2θ value, corresponding to ADD or EDD spectra, respectively. By choosing the intensities at various 2θ values for certain fixed energies (wavelengths), a series of ADD patterns, Int(E = const., 2θ), are obtained. These data are fit using the Rietveld refinement software package *GSAS* (Larson & Von Dreele, 2000; Toby, 2001). For the data collected at the APS, a polarization ratio of 0.95 is used, as the diffraction scan was in the vertical plane. The scans performed at SPring-8 were in the horizontal plane; an initial polarization ratio of 0.5 was used in the refinement. However, the refinement results are not sensitive to the parameter, because the 2θ range was limited to within $12°$.

(a)

(b)

(c)
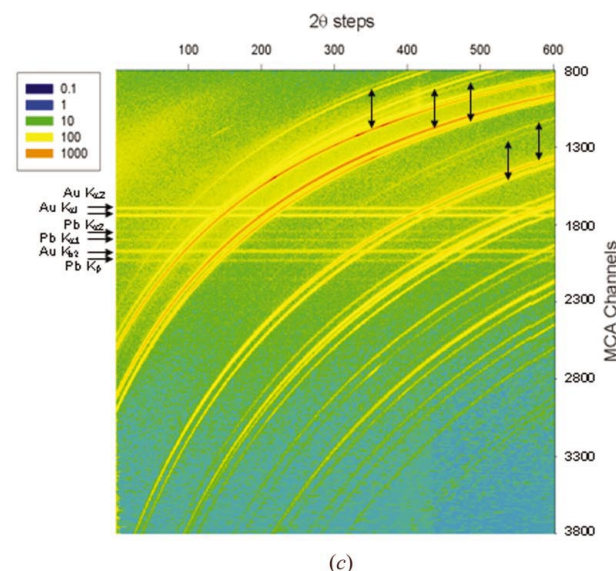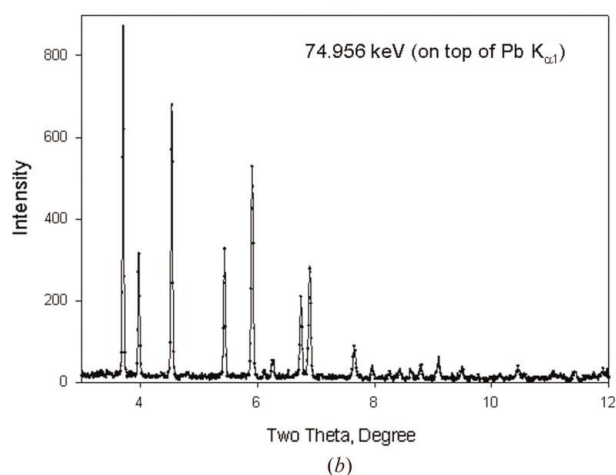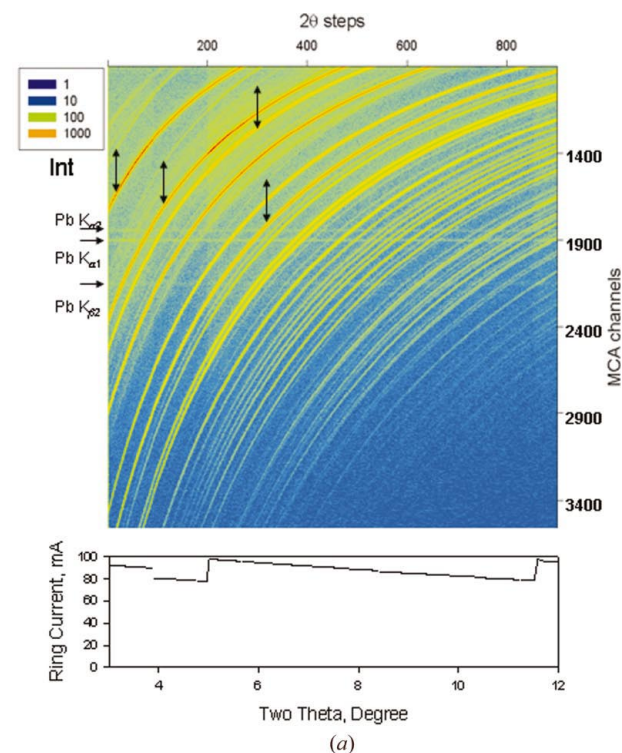
3.2. Single-wavelength refinement

Fig. 3 shows the results from an analysis by fitting a spectrum with a photon energy of 67.30 keV (MCA channel 800), corresponding to a wavelength of 0.1842 Å. The residuals R_p and wR_p for the fit are 0.164 and 0.189, respectively. The first residual is defined as $R_p = \sum |I_o - I_c| / \sum I_o$, where I_o and I_c are the observed and calculated intensities, respectively. The weighted residual, wR_p, is defined as $(wR_p)^2 = [\sum w(I_o - I_c)^2]/(\sum wI_o^2)$, where w is the weight assigned to the observed intensity (Larson & Von Dreele, 2000). The residuals are high for two reasons. Firstly, the APS mechanical 2θ drive has some systematic errors, which can be seen by the misfit of the diffraction peaks. Secondly and more importantly, the background of the ADD spectra is generally very low; hence the residuals for the background fit are generally high (often as high as 50%), resulting in elevated overall fitting residuals.

In this and all of the following fits, the observed intensities were corrected for the volume of crystallites that were present in a diffraction volume at a given 2θ. This correction is necessary because in the ambient test the size of the sample is much larger than the diffracting volume defined by the incident and diffraction beam size. Since the diffraction volume is inversely proportional to $\sin(2\theta)$, the intensity is corrected by multiplying $\sin(2\theta)$ and an arbitrary constant (typically 50). These corrections are also applied to the weights used for each profile point in the Rietveld refinement.

Note that the background of each ADD pattern is quite flat, despite the source intensity variation as a function of energy seen in the EDD patterns. These data were collected while the APS was operating at the top-up mode, which maintained a constant ring current throughout the data collection. Thus, although the I_0 value for each energy is unknown, it remained a constant and is accommodated by the scale factor in a Rietveld refinement.

3.3. Global fit to multiple wavelengths

Because an SSD can record data from a wide range of photon energies simultaneously, it is advantageous to utilize

Figure 2
(a) A plot of intensity collected on Al_2O_3 at SPring-8 against MCA channel numbers and 2θ steps (step 0 corresponds to $2\theta = 3°$, step size = $0.01°$). Note the relatively smooth background compared with that for the undulator data (Fig. 1a). The Ge escape peaks are tied to their parent peaks by arrows (from parent peak to escape). Three MCA channel regions exhibit consistently higher intensities (around channels 1844, 1899 and 2150), which arise from the Pb $K\alpha_2$ (72.794 keV), Pb $K\alpha_1$ (74.956 keV) and Pb $K\beta$ (84.9 keV) fluorescence peaks. (b) An ADD plot of data collected at SPring-8, at an energy of 74.956 keV (the Pb $K\alpha_1$ fluorescence line), MCA channel 1899. Raw data without any correction. The fluorescence line elevates the background intensity but does not affect data quality. (c) A two-dimensional plot of intensities collected on MgO + Au against MCA channel numbers and 2θ steps (step 0 corresponds to $2\theta = 3°$, step size = $0.01°$). Six MCA channel regions exhibit consistently higher intensities near 1694, 1741, 1843, 1898, 2035 and 2150, corresponding to the fluorescence peaks Au $K\alpha_2$ (66.9895 keV), $K\alpha_1$ (68.8037 keV), Pb $K\alpha_2$ (72.794 keV), Pb $K\alpha_1$ (74.956 keV), Au $K\beta_2$ (80.03 keV) and Pb $K\beta$ (84.9 keV), respectively.

research papers

Table 1
Rietveld refinement results of a combined fit to data at three wavelengths.
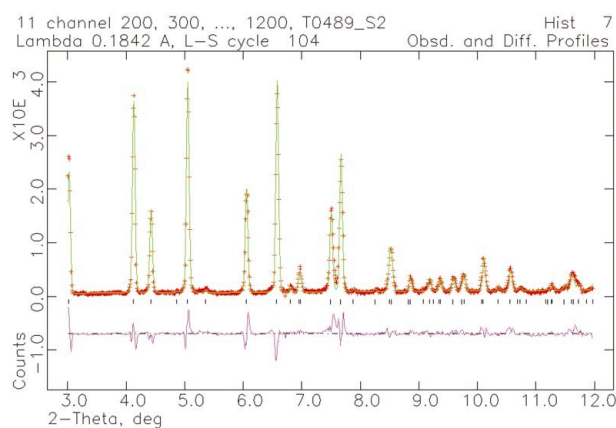
The resulting atomic positions are Al [0, 0, 0.35 (1)] and O [030 (1), 0, 0.25], with cell parameters a = 4.7667 (2) Å and c = 13.0127 (9) Å. For comparison, the NIST parameters are Al [0, 0, 0.35216 (1)], O [0.30624 (4), 0, 0.25], a = 4.7602 (4) Å and c = 12.993 (2) Å (Oetzel & Heger, 1999). See Figs. 4(a)–4(c) for visual examination of the fit. Variation in the scaling factor represents relative source spectrum intensity variation as a function of energy, as well as SSD sensitivity to photons at higher energies.

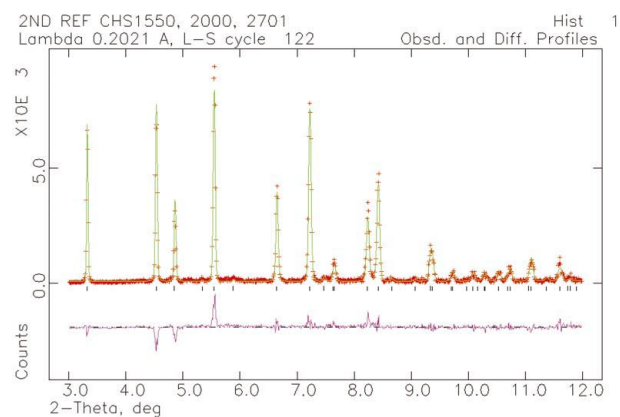| Wavelength (Å)	Energy (keV)	Scaling factor	wR_P	R_P
0.202097	61.3469	0.7139	0.233	0.169
0.157045	78.4956	0.1913	0.286	0.182
0.116565	106.3610	0.0275	0.382	0.272
Overall			0.266	0.189

multiple wavelengths for structural refinement for better coverage. For the limited 2θ range of the scans performed in this study (3–12°), 40 keV (λ = 0.310 Å) radiation covers a d-spacing range of 5.92–1.48 Å, whereas 120 keV (0.103 Å) radiation covers 1.97–0.49 Å. This increase in Q range is particularly beneficial for studies where X-ray access is limited.

Figs. 4(a)–4(c) show selected examples of a global fit of multiple wavelengths. An ideal global fit would involve all the wavelengths collected; however, the current *GSAS* package does not handle more than 99 separate 2θ scans. Thus, we selected a few wavelengths to test the feasibility of a global fit. Here data at several wavelengths are fit, together with the unit-cell parameters and atomic positions as global variables, *i.e.* they are forced to be identical for data at all wavelengths. The polarization parameter is fixed at 0.5. A forced variation from 0.3 to 0.95 does not change the fitting results significantly. Table 1 gives the quantitative fitting results and the values for alumina given by Oetzel & Heger (1999). The refined scale factors reflect a combination of several parameters: the source intensity as a function of photon energy, the absorption effects, which are strongly dependent on photon energy, and the energy dependence of the solid-state detector efficiency. On
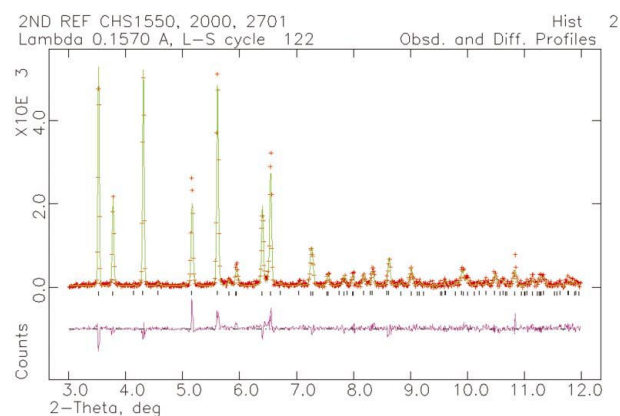
the other hand, angular dependence of the absorption is not significant because of the small 2θ range and relatively high energies used. A linear absorption coefficient is used in the fit.
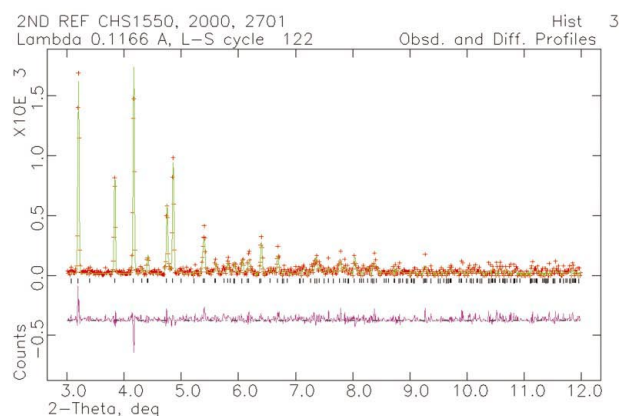

(a)

(b)

(c)

Figure 4
(a) An example of a global fit on multiple-wavelength data: 61.35 keV (0.2021 Å), MCA channel 1550. Both unit-cell parameters and atomic positions were treated as global variables in the fit. (b) An example of a simultaneous fit on multiple-wavelength data: 78.95 keV (0.1570 Å), MCA channel 2000. (c) An example of a simultaneous fit on multiple-wavelength data: 106.36 keV (0.1166 Å), MCA channel 2700. Data from SPring-8.

Figure 3
An example of a Rietveld refinement on a single-wavelength (0.1842 Å) spectrum. Data obtained from the APS, MCA channel 800.

electronic reprint

3.4. Energy 'binning' for improved angle coverage

The dense redundant data coverage allows coarser step scans while still maintaining reasonable 2θ coverage, because data in adjacent energy channels can be binned to enhance 2θ coverage. According to Bragg's law, (1), for a given d value, the angular difference $\Delta\theta$ observed at two photon energies (or wavelengths) is related by the following equation:

$$\Delta\theta = \tan\theta \, \Delta\lambda/\lambda, \qquad (2)$$

where $\Delta\lambda$ is the difference between the two wavelengths. Equation (2) can be used to convert observations at various energies to a specific wavelength.

To demonstrate this process, we first bin a data subset within a small energy range. Fig. 5 shows an example of binning the APS data centered at channel 700 (wavelength 0.2022 Å) with data from five channels: 690, 695, 700, 705 and 710. After applying (2) to convert data from channels 690, 695, 705 and 710 to channel 700, we have a five times denser 2θ coverage.
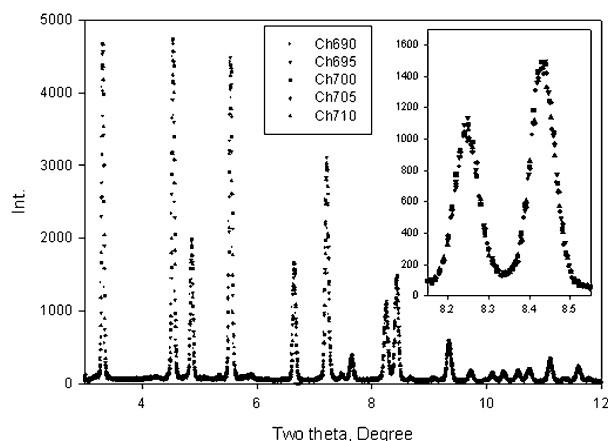

Figure 5
An example of ADD spectra obtained at the APS, showing the result of five-channel binning by applying (2). In this example, five channels, 690, 695, 700, 705 and 710, are binned to channel 700 ($\lambda = 0.2022$ Å). The inset shows two peaks near 8.35°, demonstrating the consistency of data at different channels (energies).
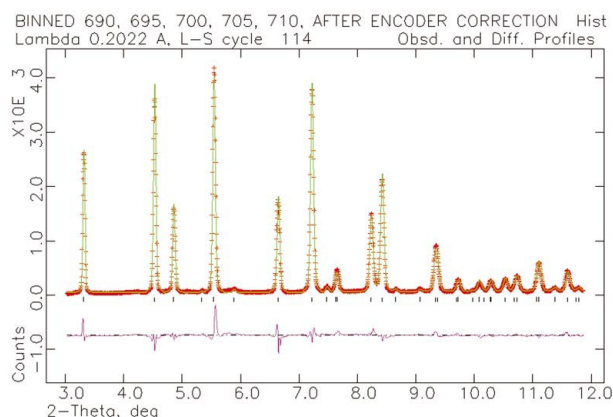

Figure 6
Rietveld refinement results for the binned data shown in Fig. 5. The wR_p value is 0.115.

The inset of Fig. 5 illustrates interconsistency of the wavelength conversion. Data from various channels fall nicely into a smooth peak profile. A slight complication is that the diffraction data after this energy binning have an uneven 2θ increment, not directly suitable for Rietveld refinement. This problem can be easily circumvented by interpolating the data at equal 2θ steps. Fig. 6 shows the interpolated data and fitting results using *GSAS*.

The binning is useful in more rapid data collection using the CAESAR technique, without losing angular resolution. According to (2), for small 2θ angles in our test,

$$\Delta\theta/\theta \simeq \Delta\lambda/\lambda. \qquad (3)$$

For a coarse step size corresponding to $\Delta\theta/\theta = 0.01$–0.1 (*i.e.* scans from 1 to 10° with a step size of 0.1°), we need to combine an energy range corresponding to a total wavelength span of $\Delta\lambda/\lambda = \Delta E/E = 0.1$ to ensure enough data density and resolution for structural refinement. To demonstrate, we select a subgroup of the EDD spectra collected at 3.0, 3.1, 3.2, 3.3, . . . , 12.0°, to simulate a scan with a 0.1° step size, ten times the actual step size. We used data from SPring-8 for this test without any intensity correction, because the bending magnet background in this data set is less variable. In principle, the effects of background can be removed, and data collected with strongly varying background can also be used for this purpose. We chose an energy range of 73.94–81.57 keV, centered at 77.75 keV, corresponding to $\Delta E/E \simeq \pm0.05$. There are 200 channels of data in this energy range in each EDD spectrum and we used only 40 data points at a five-channel increment for this demonstration.

Fig. 7 depicts the impact of energy binning on peak width by comparing data from a single-energy spectrum at 77.75 keV, with binned profiles. Compared with a single monochromatic 2θ scan at 0.01° step size, the binned data density in 2θ is
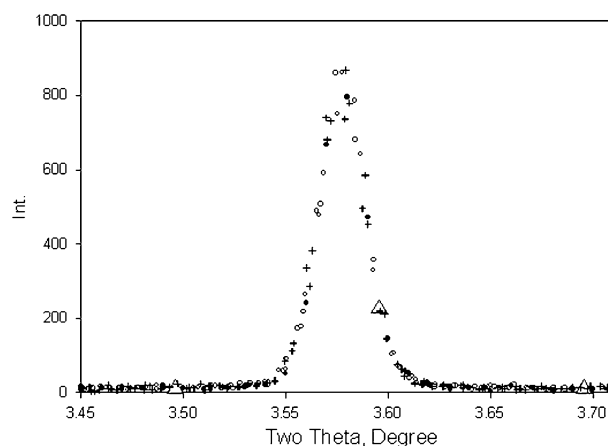

Figure 7
A comparison of peak width of a single-energy spectrum (0.01° step size) at 77.75 keV (solid circles) with the same peak after binning 40 channel data that are within ±5% of this photon energy, with a step size of 0.1° (open circles), and binning 80 channel data within ±10% of this energy, with a step size of 0.2° (crosses). The binned data have a denser angle coverage, with no significant increase in peak width. For comparison, a single-energy (77.65 keV) 0.1° step scan has only three points in this 2θ range across the peak (large open triangles).

increased by a factor of 10, despite a coarser step size of 0.1°. Note that we only binned one-fifth of the available energies in a $\Delta E/E \simeq \pm 0.05$ range. Even when the step size is increased to 0.2°, a reasonable 2θ coverage can still be achieved by binning data with the wider energy range of $\Delta E/E \simeq \pm 0.10$, although variations in background become more important. Furthermore, no significant increase in peak width is observed, suggesting that we have not compromised resolution in 2θ. From this simple analysis, we conclude that binning at the $\pm 10\%$ energy level does not significantly affect data quality.

The binned data shown in Fig. 7 are interpolated into equal 2θ steps before performing the Rietveld refinement. Fig. 8 shows the fit, with a resulting wR_p value of 0.12. Based on this analysis, we conclude that a reasonable structural refinement can be obtained using 0.1° or even 0.2° step sizes. For a 50 s EDD data collection, approximately 40 min would be required for a complete 2θ scan from 3 to 12° with a step size of 0.2°. Note that the 50 s collection time was based on less than 5% dead time and over 1000 counts per channel for the average peak intensity. With properly configured electronics and a strong incident beam, it is possible to reduce this time by a factor of 5–10, making it feasible to collect monochromatic data within 10 min.

In Fig. 9, we compare fitted peak widths, expressed as FWHM as a function of 2θ angle, between a single-wavelength ADD (at $E = 77.75$ keV) and the binned ADD (Fig. 8). The FWHM values are calculated on the basis of the well known expression originally proposed by Caglioti et al. (1958):

$$\text{FWHM} = U\tan^2\theta + V\tan\theta + W, \qquad (4)$$

where U, V and W are described by Caglioti et al. (1958) and are treated as fitting parameters in GSAS. Both the Gaussian (GU, GV and GW) and the Lorentzian (Lx and Ly) components are refined in our analysis, but only the Gaussian widths are plotted in Fig. 9, since these are generally considered to represent instrument characteristics. The Lorentzian components, which reflect particle size and microstrain in the sample, do not contribute significantly to the instrumental FWHM.
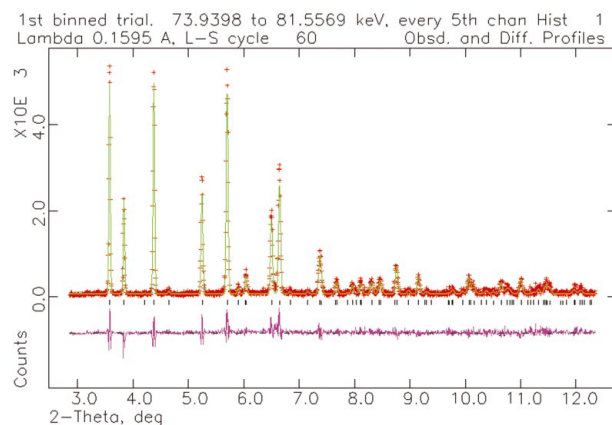

Figure 8
Rietveld refinement of a simulated 0.1° step scan, after binning the data from 73.94 to 81.56 keV, centered at 77.75 keV (wavelength = 0.1595 Å). A total of 41 channels are used, corresponding to MCA channels from 1873 to 2068, at a five-channel increment. The wR_p value is 0.12.

The Gaussian FWHM values obtained for the two binning schemes are virtually identical, varying almost linearly from $\sim 0.025°$ at $2\theta = 3°$ to $\sim 0.065°$ at $2\theta = 11°$.

To understand the origin of the observed peak width, we examine the detector resolution, which was determined on the basis of the FWHM of two characteristic isotope decay lines at 5.9 keV (Fe^{55}) and 122.06 keV (Co^{57} γ_2). Typical calibrations show that the energy resolution varies from 140 eV at 5.9 keV to 490 eV at 122.06 keV, corresponding to $\Delta E/E$ of 0.0237 and 0.0040, respectively. Assuming that $\Delta E/E$ varies with the square root of E, at 77.65 keV the resolution $\Delta E/E$ is about 0.005. Further assuming that this $\Delta E/E$ represents the energy discrimination in the CAESAR technique, from (3), the width of a given diffraction peak (FWHM expressed in $2\Delta\theta$) is related to $\Delta E/E$ by

$$2\Delta\theta = 2(180/\pi)\tan\theta\,\Delta E/E. \qquad (5)$$

The long-dashed line in Fig. 9 shows that the peak width predicted by (5) is consistent with the angular dependence observed in the sample FWHM, which is about 25% worse than the detector energy resolution (without considering the effects of beam collimating optics) or about 0.006 at 77.65 keV.

3.5. High-pressure test

The small sample diameter under high pressure requires an intensity correction scheme that differs from the simple corrections described in previous sections. The incident (subscript i) and diffracted (subscript d) beam widths (measured in the direction perpendicular to the sample cylindrical axis) are defined by the beam collimating slits to be $w_i = w_d = 0.05$ mm. At low angles, the length of the diffracting volume in the direction parallel to the incident beam, $L = w_i/\tan(2\theta) + w_d/\sin(2\theta)$, may exceed the sample diameter, D. Assuming that the center of the diffracting volume coincides
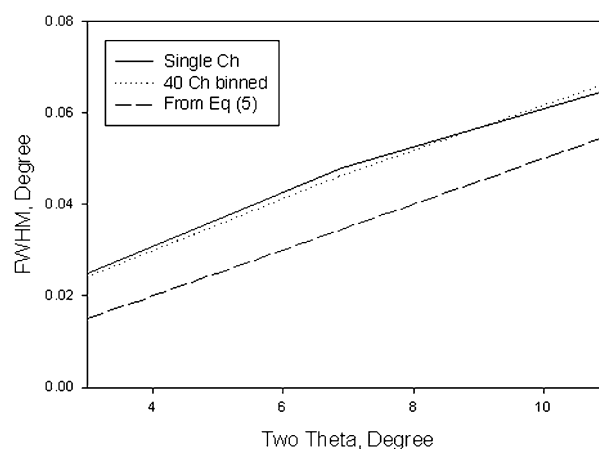

Figure 9
FWHM of diffraction peaks (in °) as a function of 2θ for data collected at SPring-8. The dotted line is the result of fitting data at a single wavelength ($E = 77.65$ keV); the solid line is for binned data using 40 different photon energies from 73.94 to 81.56 keV (Fig. 8). The long-dashed line represents the predicted angular resolution limit due to energy resolution of the solid-state detector, based on FWHM measurements on characteristic radioactive decay lines, based on (5).

with the cylindrical axis of the sample (this is achieved by scanning the sample by moving the press so that the diffraction signals are maximized), the following correction scheme is used to scale observed intensities to a constant diffracting volume:

$$I_c = C\,I_o\,\sin(2\theta)/(w_i w_d)$$

when $L \leq D$ and

$$I_c = C\,I_o\,/\,[(w_i w_d)\,/\,\sin(2\theta) - (L - D)^2 \tan(2\theta)/4]$$

when $L \leq D$. Fig. 10 shows an example of Reitveld refinement on the high-pressure data collected on MgO and Au, after binning 23 channels centered at channel 2298 ($\lambda = 0.1368$ Å, $E = 90.600$ keV) with data from channels 2243–2343 at five-channel steps: 2243, 2248, 2253, . . . , 2353, corresponding to energies from 88.45 to 92.75 keV. The data have been interpolated at equal 2θ steps. The fitted residuals are $R_p = 0.180$ and $wR_p = 0.226$, and the refined molar contents for MgO and Au are 89 (1) and 11 (1)%, respectively.

We have demonstrated that a $0.2°$ step size is also sufficient for high-pressure data collection, corresponding to an effective data collection time of about 20 min. Details of the high-pressure data collection and analysis are given in a separate paper (Wang *et al.*, 2004).

4. Conclusions

We have demonstrated the feasibility of the CAESAR technique, which can be applied to any diffraction experiments that have limited X-ray access to the sample, including the multianvil press and the diamond anvil cell, to facilitate fast data collection. In certain high-pressure devices the sample can be rotated along an axis parallel to the 2θ rotation axis, thereby reducing the effects of preferred orientation.

This technique is not limited to high-pressure studies; it is applicable to essentially all synchrotron-related diffraction studies by collecting diffraction information from all available photons. The technique has certain advantages over conventional monochromatic X-ray diffraction methods.
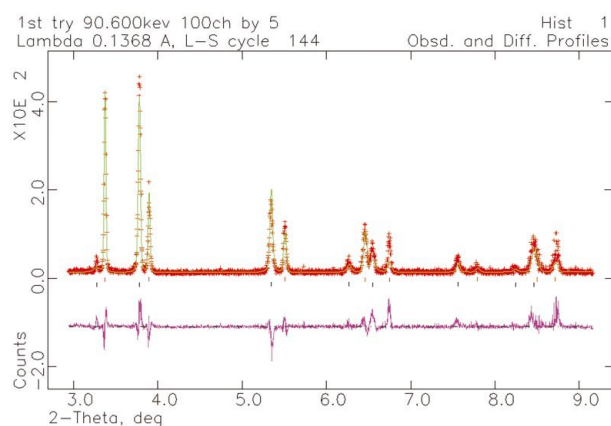

Figure 10
Rietveld refinement results for the binned data set for a mixture of MgO and Au at 8 GPa (Fig. 3c). The upper row of ticks indicates Au peak positions and the lower row of ticks MgO. $R_p = 0.17$, $wR_p = 0.22$.

(i) This technique does not require a monochromator, and X-rays at very high energies (over 100 keV) in the white-beam spectrum can be used to obtain angle-dispersive data.

(ii) Incident and diffracted collimators define a prescribed diffracting volume, thereby eliminating the problems of background, which are present in typical two-dimensional monochromatic diffraction measurements.

(iii) Energy-dependent background in the energy-dispersive spectrum caused by the source may be eliminated (as far as background is not dependent on angle) when the data are regrouped into constant-energy scans. Even if the diffraction peaks in EDD data overlap with a fluorescent line at E_f, the ADD data Int($E = E_f$, 2θ) remains unaffected by this overlap, because the intensity of fluorescent lines should remain constant at all angles.

(iv) Data from multiple energies can be binned to increase effective 2θ or Q coverage and to improve counting statistics; hence scan steps can be significantly increased and thus this technique can be significantly less time consuming than a traditional step-scan monochromatic diffraction measurement. Our test results indicate that even when a wide energy of $\Delta E/E \simeq \pm0.10$ is used in the binning, no significant peak width broadening is observed.

(v) This technique allows for flexibility in switching between ED and AD modes. Monochromatic data collections are generally more time consuming, while energy-dispersive data cannot give reliable structural information. Using the CAESAR technique, one can collect high-pressure data in the ED mode without a 2θ scan to obtain information quickly, such as pressure and phase identification. At a critical point under certain pressure and temperature conditions, one can then conduct a step scan to collect angle-dispersive data. This allows one to take advantage of both energy-dispersive and angle-dispersive methods.

References

Angel, R. J., Downs, R. T. & Finger, L. W. (2000). *High-Temperature and High-Pressure Crystal Chemistry*, edited by R. M. Hazen & R. T. Downs, pp. 559–596. Washington, DC: Mineralogical Society of America.

Ballirano, P. & Caminti, R. (2001). *J. Appl. Cryst.* **34**, 757–762.

Caglioti, G., Paoletti, A. & Ricci, F. P. (1958). *Nucl. Instrum. Methods*, **35**, 223–228.

Larson, A. C. & Von Dreele, R. B. (2000). *General Structure Analysis System* (*GSAS*). Report LAUR 86-748. Los Alamos National Laboratory, New Mexico, USA.

Oetzel, M. & Heger, G. (1999). *J. Appl. Cryst.* **32**, 799–807.

Schulze, C. & Kleuker, U. (1998). *J. Synchrotron Rad.* **5**, 1085–1087.

Shim, S.-H., Duffy, T. S. & Takemura, T. (2002). *Earth Plant. Sci. Lett.* **203**, 729–739.

Speziale, S., Zha, C.-S., Duffy, T. S., Hemley, R. J. & Mao, H.-K. (2001). *J. Geophys. Res.* **106**, 515–528.

Toby, B. H. (2001). *J. Appl. Cryst.* **34**, 210–213.

Uchida, T., Wang, Y., Rivers, M. L. & Sutton, S. R. (2001). *J. Geophys. Res.* **106**, 21799–21810.

Urakawa, S., Igawa, N., Umesaki, N., Igarashi, K., Shimomura, O. & Ohno, H. (1996). *High Pressure Res.* **14**, 375–382.

Utsumi, W., Funakoshi, K., Urakawa, S., Yamakata, M., Tsuji, K., Konishi, H. & Shimomura, O. (1998). *Rev. High Pressure Sci. Technol.* **7**, 1484–1486.

Wang, Y., Rivers, M., Uchida, T., Murray, P., Shen, G., Sutton, S., Chen, J., Xu, Y. & Weidner, D. (2000). *Proceedings of the International Conference on High Pressure Science and Technology (AIRAPT-17), Science and Technology of High Pressure*, Vol. 2, pp. 1047–1052. Hyderabad: Universities Press (India).

Wang, Y., Uchida, T., Von Dreele, R. B., Nishiyama, N., Nozawa, A., Funakoshi, K. & Kaneko, H. (2004). *Reviews for Frontiers of High Pressure Research: Geophysical Applications*, edited by J. Chen, Y. Wang, T. S. Duffy, G. Shen & L. Dubritsinskaya. New York: Elsevier. In the press.

Yamanaka, T. & Ogata, K. (1991). *J. Appl. Cryst.* **24**, 111–118.

Yamanaka, T., Sugiyama, K. & Ogata, K. (1992). *J. Appl. Cryst.* **25**, 11–15.

Yaoita, K., Katayama, Y., Tsuiji, K., Kikegawa, T. & Shimomura, O. (1997). *Rev. Sci. Instrum.* **68**, 2106–2110.

Zhao, Y., Parize, J. B., Wang, Y., Kusaba, K., Vaughan, M. T., Weidner, D. J., Kikegawa, T., Chen, J. & Shimomura, O. (1994). *Am. Mineral.* **79**, 615–621.